Imperfections and optical absorption in glow-discharge *a*-Si:H films: A study in the visible and near-infrared region

A. Kondilis
Department of Physics, University of Crete, P.O. Box 2208, 71003 Heraklion, Greece
(Received 14 August 1998; revised manuscript received 18 April 2000)

In the present work, we study the effect of imperfections on the optical spectra of glow-discharge *a*-Si:H films in detail. Important features manifested in experimental power-loss and reflectance optical spectra are given a clear interpretation. Taking imperfections properly into account, we develop an optical method of analysis by which the absorption coefficient is extracted down to $\sim 10\ \mathrm{cm}^{-1}$, a significant improvement over conventional optical methods, which hardly reach $10^2\ \mathrm{cm}^{-1}$. The results are in good agreement with the results of photothermal deflection spectroscopy (PDS) and the constant photocurrent method (CPM). If measurements are to be performed at different temperatures, this optical method is important, since the temperature range of safe use of PDS and CPM is appreciably limited.

I. INTRODUCTION

Native imperfections, which inevitably accompany the fabrication of a film, crucially affect the optical spectra in the visible and near-infrared region, the range of interest to this study. However, in analyzing spectra, it is a common practice to neglect imperfections and employ the standard model of an ideal sample. This simplification is often a poor approximation to actual samples that fails to interpret important features in the spectra. In addition, in extracting the absorption coefficient, it produces false absorption tails, thus providing a poor knowledge of the absorption edge.

Despite many publications[1–5] on imperfections, there is no work to our knowledge that effectively treats the foregoing failings of the optical analysis. In the present work, aiming at an improved analysis, we proceed to an examination of imperfections in detail. Even though developed for *a*-Si:H films, this study is appraised to have a more general value that goes beyond the scope of the specific considerations.

To deal with imperfections, we have developed models by which surface roughness and nonparallel interfaces as well as the inhomogeneous material properties are properly taken into account. Within these models, important features manifested in reflectance and power-loss experimental spectra are given a clear interpretation. Applying this understanding of the role of imperfections, we have also developed an optical method of analysis. The method allows us to extract the absorption coefficient down to $\sim 10\ \mathrm{cm}^{-1}$, while conventional optical methods hardly reach $10^2\ \mathrm{cm}^{-1}$. Good agreement with the results of photothermal deflection spectroscopy[6] (PDS) and the constant photocurrent method[7] (CPM) is verified at room temperatures, thus lending support to the optical method developed.

It is important to stress that successful utilization of the proposed method does not depend on the temperature at which measurements are to be performed. This is a great advantage over the CPM and PDS, which lack this important property. The necessity of a thermally index-sensitive deflecting medium, as well as the requirement of lack of any nonuniform heating-induced turbulence in that medium, place a serious constraint[8] on utilization of PDS for measurements at different temperatures. The CPM fails[9] between 80 and 200 K: In this temperature range, the Rose factor depends on the photon energy, thus violating an important CPM rule.

The safe use of the proposed optical method at any temperature has proved catalytic for successfully measuring the thermal variation of the Urbach absorption edge in *a*-Si:H. The results, to be presented in a forthcoming paper,[10] challenge the widely accepted view[11] suggested by Cody. On the one hand, the Urbach edge appears to be far less sensitive to temperature than suggested in Ref. 11. On the other hand, the Urbach focus is detected at 3.3 and not at 2.1 eV. The former value, unlike the latter, is quite close to 3.5 eV, the energy corresponding to the first direct optical transition in *c*-Si. This result bridges a large discrepancy between theory and experiment, since theory does predict[11] an Urbach focus at this very energy.

The present study is organized into three main sections. In Sec. II we consider the effect of imperfections on reflectance spectra and in Sec. III their effect on power-loss spectra. Finally, in Sec. IV we present and examine the efficiency of our optical method of analysis.

II. REFLECTANCE SPECTRA IN THE PRESENCE OF IMPERFECTIONS

A. Analytical and numerical treatment of reflectance

In this section, we calculate reflectance, dealing with imperfections in terms of normal inhomogeneity and lateral inhomogeneity. By normal inhomogeneity, we mean changes that occur in the properties of the film along the z direction, the direction of growth. Such changes are due to the formation of thin layers, inhomogeneity layers, which grow at the ends of the film during fabrication. Inhomogeneity layers differ from the bulk in composition and structure. Experimental evidence from hydrogen profiling experiments[12] shows that their typical size is 100 nm. By lateral inhomogeneity, we mean changes that occur in the properties of the film in the directions x and y, the directions normal to the

direction of growth. Such changes are due to either the geometry of the interfaces or the microstructure inside the film. Nonparallel interfaces and surface roughness, as well as scatterers with typical sizes that range from 1 to 10 nm (like voids, microcrystallites, islands of material with different properties from the rest of the bulk, etc.), constitute a variety of factors that give rise to lateral inhomogeneity.

We model the foregoing two types of imperfection as follows. In dealing with normal inhomogeneity, we consider the bulk of the film embedded between two inhomogeneity layers; one near the free surface of the film and another near the interface with the substrate. For obvious reasons we call the former a front inhomogeneity layer (FIL) and the latter a back inhomogeneity layer (BIL). Let n_{FIL} be the refractive index of the FIL, n_{bulk} that of the bulk, n_{BIL} that of the BIL, and n_{subs} that of the substrate. These indices, along with the respective layer thicknesses D_{FIL}, D_{bulk}, D_{BIL}, and D_{subs} form a particular index profile. To calculate the reflectance R^z for this particular profile, we employ the transfer matrix method.[3] The finite size of the film produces fringes in the calculated R^z spectra, which are decorated, however, with finer fringes produced by the finite substrate. In any experiment, the wavelength resolution of the light beam incident on the film cannot be so fine as to allow the substrate fringes to be detected, and, in fact, they need not be detected. In the calculations, we take this into account by averaging them out.[13]

In dealing with lateral inhomogeneity, we consider that the only effect it produces is phase incoherence induced by small optical-thickness variations. As long as lateral inhomogeneity is missing, l, the optical thickness[3] of the film, has a definite value $L=n_{\mathrm{FIL}}D_{\mathrm{FIL}}+n_{\mathrm{bulk}}D_{\mathrm{bulk}}+n_{\mathrm{BIL}}D_{\mathrm{BIL}}$. The same is also true for φ, the phase thickness[3] of the film. As φ bears a simple relation to l, $\varphi=2\pi(E/hc)l$, its definite value is

$$\Phi=2\pi\frac{E}{hc}L, \tag{1a}$$

where E is the photon energy, h Planck's constant, and c the speed of light. Upon introducing lateral inhomogeneity, we treat l and, as a consequence φ, as randomly varying quantities. Let us consider l to be uniformly distributed about L: $l=L\pm\Delta l$. Then φ is also uniformly distributed about Φ: $\varphi=\Phi\pm\Delta\varphi$, where

$$\Delta\varphi=2\pi\frac{E}{hc}\Delta l. \tag{1b}$$

The resulting incoherence-induced effect on reflectance is taken into account by the following averaging:

$$R(\Phi)=\frac{1}{2\Delta\varphi}\int_{\Phi-\Delta\varphi}^{\Phi+\Delta\varphi}R^z(\varphi)d\varphi. \tag{1c}$$

It should be noted that in Eq. (1c) integration is performed only over the total phase thickness of the film. All other parameters are kept constant upon integration.

The averaging given by Eq. (1c), along with the transfer matrix method employed in the calculation of R^z, provide a handy mathematical tool for performing numerical simulations. However, one cannot disregard the value of an analytical treatment in that it always favors a direct and clear insight into the effects studied. As we shall see below, inhomogeneity, either normal or lateral, crucially affects reflectance spectra and, especially, their envelopes. Prompted by this, we have derived approximate analytical expressions for reflectance envelopes. The derivation is as follows.

First, taking $\Delta\varphi$ small as compared to the width of one fringe, i.e., for $\Delta\varphi\ll\pi$, we cast Eq. (1c) into the form

$$R(\Phi)=R^z(\Phi)+\frac{1}{6}\frac{\partial^2R^z(\Phi)}{\partial\varphi^2}\Delta\varphi^2. \tag{2}$$

The first term is the contribution of normal inhomogeneity and the second term the contribution of lateral inhomogeneity. Then, assuming that the moduli of the Fresnel reflection coefficients[3] $r_{\mathrm{bulk/FIL}}$ and $r_{\mathrm{bulk/BIL}}$ are small compared to unity, we derive R^z. Finally, applying the ordinary conditions for interference extrema to Eq. (2), we obtain the reflectance-maxima envelope $R_{\max}$ and the reflectance-minima envelope $R_{\min}$. In particular, we apply the condition $\{\Phi=q\pi+\pi/2,\ q\in N\}$ to obtain $R_{\max}$ and the condition $\{\Phi=q\pi,\ q\in N\}$ to obtain $R_{\min}$. Aiming at a clearer understanding of the inhomogeneity-induced effects, we have omitted absorption in the foregoing derivation. Our assumptions $\Delta\varphi\ll\pi$, $|r_{\mathrm{bulk/FIL}}|\ll1$, and $|r_{\mathrm{bulk/BIL}}|\ll1$ are justified for the systems studied.

The analytical expressions derived for $R_{\max}$ and $R_{\min}$ are

$$R_{\max}=R^z_{\max}-C^z[(1-R^z_{\max})\Delta\varphi]^2 \tag{3a}$$

and

$$R_{\min}=R^z_{\min}+C^z[(1-R^z_{\min})\Delta\varphi]^2. \tag{3b}$$

The net contribution of normal inhomogeneity reads

$$R^z_{\max}=1-\frac{4x_1n_{\mathrm{subs}}}{(1+x_1)(n^2_{\mathrm{subs}}+x_1)}+\frac{8x_1n_{\mathrm{subs}}(x_1^2-n^2_{\mathrm{subs}})}{(1+x_1)^2(n^2_{\mathrm{subs}}+x_1)^2}\times\{O_{\mathrm{FIL}}+O_{\mathrm{BIL}}\} \tag{3c}$$

and

$$R^z_{\min}=1-\frac{4x_2n_{\mathrm{subs}}}{(1+x_2)(n^2_{\mathrm{subs}}+x_2)}+\frac{8x_2n_{\mathrm{subs}}(n^2_{\mathrm{subs}}-x_2^2)}{(1+x_2)^2(n^2_{\mathrm{subs}}+x_2)^2}\times\{O_{\mathrm{FIL}}-O_{\mathrm{BIL}}\}, \tag{3d}$$

where

$$(x_1,x_2)=\left(n_{\mathrm{BIL}}n_{\mathrm{FIL}},\frac{n_{\mathrm{BIL}}}{n_{\mathrm{FIL}}}\right), \tag{3e}$$

$$O_{\mathrm{FIL}}=r_{\mathrm{bulk/FIL}}\cos(2\Phi_{\mathrm{FIL}}), \tag{3f}$$

and

$$O_{\mathrm{BIL}}=r_{\mathrm{bulk/BIL}}\cos(2\Phi_{\mathrm{BIL}}). \tag{3g}$$

Φ_{FIL} and Φ_{BIL} are the phase thicknesses of the FIL and the BIL, respectively. The prefactor C^z present in Eqs. (3a) and (3b) in the terms of lateral inhomogeneity depends on normal inhomogeneity only. It takes the simple form

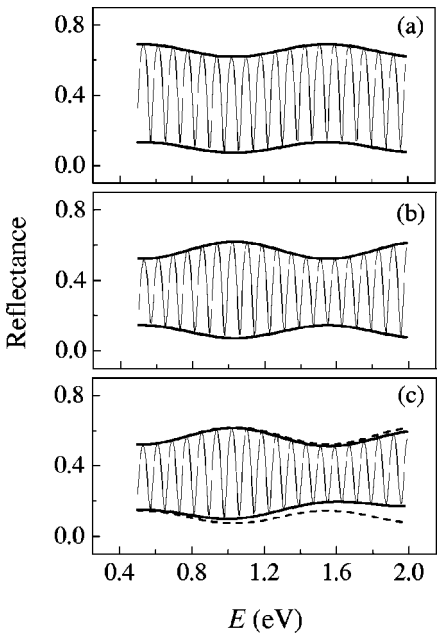

FIG. 1. Reflectance spectra in the presence of imperfections. Absorption is omitted. Full spectra, depicted by thin solid lines, are the exact numerical results of the transfer matrix method. Envelopes, depicted by bold solid lines, are the results of the approximate analytical expressions (3a)–(3h). (a) Net effect of normal inhomogeneity. The only imperfection is one front inhomogeneity layer. $n_{\mathrm{FIL}}=4$ and $D_{\mathrm{FIL}}=150$ nm. (b) Net effect of normal inhomogeneity. The only imperfection is one back inhomogeneity layer. $n_{\mathrm{BIL}}=3$ and $D_{\mathrm{BIL}}=200$ nm. (c) Combined effect of normal and lateral inhomogeneity. $\Delta l=50$ nm. Normal inhomogeneity is identical to that of (b). To have a clear view of the separate effects of normal and lateral inhomogeneity, the envelopes in the absence of lateral inhomogeneity ($\Delta l=0$) are shown as dashed lines. For all illustrated cases, $n_{\mathrm{subs}}=1.5$, $n_{\mathrm{bulk}}=3.5$, and $D_{\mathrm{bulk}}=2$ μm.

$$C^z=\frac{(x_1-x_2)(x_1x_2-n_{\mathrm{subs}}^2)}{12x_1x_2n_{\mathrm{subs}}} \tag{3h}$$

if the boundaries of the film are much more reflective than the interfaces formed inside the film between the bulk and the inhomogeneity layers.

B. Imperfection-induced effects on reflectance spectra

The net effect of normal inhomogeneity on reflectance spectra is illustrated for two particular cases in the graphs (a) and (b) of Fig. 1. Evidently, inhomogeneity layers cause the envelopes of reflectance to oscillate. Note that for an entirely homogeneous film envelopes are free of any oscillations. They are straight lines parallel to the energy axis. In the cases illustrated in Figs. 1(a) and 1(b), we observe two particular envelope oscillatory modes: in-phase oscillations and completely out-of-phase oscillations. A trivial exploration of Eqs. (3c) and (3d) reveals that final envelopes always result from the superposition of these two particular modes. More specifically, if the FIL contributes an in-phase oscillatory mode, the BIL, necessarily, contributes a completely out-of-phase oscillatory mode, and vice versa. Which of the two possibilities occurs depends on the sign of $(x_1^2-n_{\mathrm{subs}}^2)(n_{\mathrm{subs}}^2-x_2^2)$. In either of the graphs (a) and (b), only one of the foregoing two oscillatory modes survives as, in each case, only one inhomogeneity layer is considered. Inferences drawn above about envelope oscillations are valid not only in the simple case of one front-back inhomogeneity layer. It can be proved that they hold in the general case of arbitrary front-back index profiles, since, even then, Eqs. (3c) and (3d) keep the same form.

Figure 1(c) illustrates the effect of lateral inhomogeneity. In order to have a clear view, the envelopes before the introduction of lateral inhomogeneity are shown by dashed lines. As seen, interference fringes become damped. The effect is sizable on the minima. However, it is negligible on the maxima. This difference is clearly understood through the help of Eq. (1c). An R^z spectrum has fringes that are sharper around minima and broader around maxima, so the R^z values that enter the averaging of Eq. (1c) are spread within an interval that is appreciably larger in the case of the minima than it is in the case of the maxima.

Surface roughness, as a type of lateral inhomogeneity, is expected to affect reflectance in the manner seen in Fig. 1(c), but it does not. A rigorous treatment[2] of roughness predicts, not rising, but lowering of the reflectance-minima envelope. So for this particular type of lateral inhomogeneity Eq. (1c) is invalid. Anyway, for the cases of interest to this study, the typical rms height of surface irregularities is sufficiently small[14] for the effect on reflectance to be negligible and thus ignored.

The results of the approximate expressions (3a) and (3b), shown by the bold solid lines, successfully reproduce exact numerical data. Several tests, equally successful, give these expressions a validity that unambiguously covers all of the cases of interest to this study.

C. A nontrivial experimental case

In this section, we focus on the experimental spectrum of a glow-discharge a-Si:H film. The specific spectrum is shown in Fig. 2(a). Between 1.2 and 1.6 eV, in the region of low absorption, fringes are sizable. For $E>1.6$ eV, they shrink dramatically due to increasing absorption until they vanish altogether. However, what makes this particular spectrum interesting is not this expected behavior but the unusual behavior of its envelopes. As seen, the minima envelope exhibits an oscillatory behavior. On the other hand, the maxima envelope does not oscillate at all, having a constant value in the entire range of low absorption. This different behavior between minima and maxima can be explained through Eqs. (3c) and (3d). As regards maxima, the oscillatory terms originating from the FIL and BIL interfere destructively:

$$O_{\mathrm{FIL}}+O_{\mathrm{BIL}}=0. \tag{4}$$

But then, as regards minima, these terms necessarily interfere constructively, thus giving a sizable oscillation. The validity of Eq. (4) within the whole range of low absorption entails that

$$\Phi_{\mathrm{FIL}}=\Phi_{\mathrm{BIL}} \tag{5}$$

and

$$n_{\mathrm{bulk}}^2=n_{\mathrm{BIL}}n_{\mathrm{FIL}}. \tag{6}$$

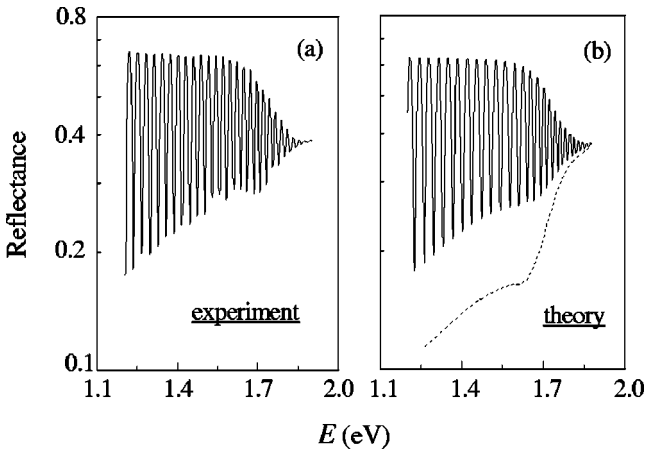

FIG. 2. (a) The experimental reflectance spectrum of a glow-discharge a-Si:H film is illustrated. (b) The theoretical reproduction of that spectrum, the solid line, is shown. For $E \leqslant 1.58$ eV, the constant index values as calculated in Sec. II C were employed. At higher energies, n_{FIL}, n_{bulk}, and n_{BIL} were given typical dispersions. The absorption coefficient used was derived in the way detailed in Sec. IV of the text. To have a clear view of the separate effects of normal and lateral inhomogeneity, the calculated minima envelope in the absence of lateral inhomogeneity is illustrated as the dashed line.

As shown in Fig. 1(c) and discussed in Sec. II B, the second term of Eq. (3a), the term of lateral inhomogeneity, produces a negligible effect on $R_{\max}$. By neglecting this term and using Eqs. (3c), (3e), (4), and (6), we obtain

$$R_{\max} = 1 - \frac{4 n_{\mathrm{bulk}}^2 n_{\mathrm{subs}}}{(1+n_{\mathrm{bulk}}^2)(n_{\mathrm{subs}}^2 + n_{\mathrm{bulk}}^2)}. \tag{7}$$

Substituting the value 1.53 for n_{subs} and the corresponding experimental value for $R_{\max}$ in Eq. (7), we calculate a frequency-independent n_{bulk} in the region of low absorption, $n_{\mathrm{bulk}} = 3.67$. This is a good approximation, since it is well known that the refractive index of a-Si:H bears a weak dependence on frequency for 1.2 eV$<E<$1.6 eV and has values very close to the one calculated.

At $E = 1.58$ eV, due to the local maximum of the experimental envelope $R_{\min}$ at this energy, it holds that

$$\cos[2\Phi_{\mathrm{FIL}}(E=1.58\,\mathrm{eV})] = -1 \Leftrightarrow \left\{ \Phi_{\mathrm{FIL}}(E=1.58\ \mathrm{eV}) = \frac{\pi}{2} + Q\pi, \quad Q \in N \right\}. \tag{8}$$

By neglecting any weak dispersion of the refractive index in the low-absorption region, we have two additional valid equations, derived from Eqs. (1c), (3b), and (8):

$$\frac{R_{\min}(E=1.20\ \mathrm{eV}) - R_{\min}^z[\Phi_{\mathrm{FIL}} = (1.20/1.58)(\pi/2 + Q\pi)]}{C^z\{1 - R_{\min}^z[\Phi_{\mathrm{FIL}} = (1.20/1.58)(\pi/2+Q\pi)]\}^2} = c_{01}\Delta l^2 \tag{9}$$

and

$$\frac{R_{\min}(E=1.58\ \mathrm{eV}) - R_{\min}^z(\Phi_{\mathrm{FIL}} = \pi/2 + Q\pi)}{C^z[1 - R_{\min}^z(\Phi_{\mathrm{FIL}} = \pi/2 + Q\pi)]^2} = c_{02}\Delta l^2, \tag{10}$$

where $c_{01} = 3.70 \times 10^{-5}\,\mathrm{nm}^{-2}$ and $c_{02} = 6.41 \times 10^{-5}\,\mathrm{nm}^{-2}$. On substituting the corresponding experimental values for $R_{\min}(E=1.20\,\mathrm{eV})$ and $R_{\min}(E=1.58\,\mathrm{eV})$, the set of Eqs. (5), (6), (9), and (10) gives multiple solutions for the inhomogeneity parameters. However, only one solution survives under specific criteria. Equation (6) implies that either $n_{\mathrm{FIL}} < n_{\mathrm{bulk}} < n_{\mathrm{BIL}}$ or $n_{\mathrm{FIL}} > n_{\mathrm{bulk}} > n_{\mathrm{BIL}}$. However, it is only with the latter combination that we obtain a physically meaningful solution. On the other hand, Q, appearing in Eq. (8), determines the number of local extrema manifested on the envelope $R_{\min}$ within a given energy range. If $Q>1$, we have, contrary to the experimental result, more than one local extremum manifested between 1.2 and 1.58 eV on the calculated envelope. If $Q=0$, the solutions obtained for n_{FIL} and n_{BIL} are meaningless. Therefore $Q=1$. The calculated indices and thicknesses of the inhomogeneity layers are $n_{\mathrm{FIL}} = 3.96$, $n_{\mathrm{BIL}} = 3.40$, $D_{\mathrm{FIL}} = 149$ nm, and $D_{\mathrm{BIL}} = 173$ nm. The calculated half width of the optical-thickness distribution $\Delta l = 68$ nm.

It is apparent in Fig. 2(b) that the foregoing parameter values reproduce the features of the experimental envelopes in all the details. To have a clear view of the separate effects of normal and lateral inhomogeneity, the calculated minima envelope in the absence of lateral inhomogeneity is shown as the dashed line. It should be noted that the wavelength spectral width of the polychromatic light incident on the film is too small ($\Delta\lambda \approx 1$ nm) to cause any measurable fringe damping.[5] Thus, it is fully justified to attribute the whole damping to intrinsic properties of the film, namely, lateral inhomogeneity.

Experimental evidence from Ref. 15 shows that the general trend is a decrease in the refractive index with increase in hydrogen concentration. In interpreting the calculated index profile exclusively in terms of hydrogen concentration, we conclude that, within a distance of 149 nm from the air/film interface, the hydrogen concentration is lower than the concentration in the bulk. This conclusion agrees with the results of other investigations,[12] which map the hydrogen concentration profile using a method based on nuclear reactions. Within 173 nm from the substrate/film interface, the material seems to be richer in hydrogen than it is in the bulk. However, such an assertion is deceptive, as the value of the refractive index near the interface with the substrate reflects not only the effect of hydrogen content but also that of lower density and nonrelaxed stresses, the latter being especially strong in this specific area.

III. POWER-LOSS SPECTRA IN THE PRESENCE OF IMPERFECTIONS

A. Methods of calculation

When light interacts with an inhomogeneous film, it dissipates power in absorption and diffuse scattering. Then the resulting loss of power P is given by

$$P = 1 - R - T, \tag{11}$$

where R and T are the reflectance and transmittance, respectively, in the so-called specular[1,2] directions. Strictly speaking, P in Eq. (11) is the loss of power normalized to the

incident power. From now on, whenever we use the term ''power,'' we mean the normalized power.

In order to derive P given in Eq. (11), we need to cope with the different factors of inhomogeneity and dissipation present in the film. Let us consider normal inhomogeneity as in Sec. II and deal with absorption through a spatially independent absorption coefficient a. At this stage, the calculated loss of power P^z is specified by this particular absorption coefficient and the particular index profile introduced by normal inhomogeneity.

Next, let us consider lateral inhomogeneity. At this stage, special attention is required as this patricular type of inhomogeneity needs special treatment. Lateral inhomogeneity, through the microstructure inside the film and the surface roughness, dissipates power in diffuse scattering. In good-quality glow-discharge a-Si:H films, and in the wavelength range of interest to this study, the microstructure dissipates negligible[16,17] power. Thus, the only underlying reason for diffuse scattering is surface roughness. In taking this into account, we deal with the two foregoing factors of lateral inhomogeneity in different ways. While we tackle the microstructure just as a φ incoherence source through an averaging similar to that of Eq. (1c), we treat surface roughness as a diffuse-scattering source through the employment of scalar diffraction theory.[2] One should note that a φ incoherence treatment like that of Eq. (1c) is a power-nondissipative operation in itself. As such, it is inadequate to account for any diffuse-scattering losses and thus inappropriate to represent the effect of roughness. The calculated loss of power $P^{z,\sigma}$ derived from applying scalar diffraction theory to all three interfaces of the film-substrate system considered is given by

$$P^{z,\sigma}=P^z+D_1^z\sigma_1^2+D_2^z\sigma_2^2+D_3^z\sigma_3^2. \tag{12}$$

σ stands for the rms height of surface irregularities. The subscript 1 labels the air/film interface, subscript 2 the film/substrate interface, and subscript 3 the substrate/air interface. The derivation of Eq. (12) presupposes that $\{\sigma_j/\lambda \ll 1,\ j=1,2,3\}$, where λ is the wavelength of light. On the other hand, for a scalar approach to be valid, the radius of curvature of surface irregularities should be much larger than the wavelength of light. This entails that $\{\lambda\sigma_j/\xi_j^2 \ll 1,\ j=1,2,3\}$, where ξ_j is the autocorrelation length of surface irregularities at interface j. For typical values[14] of the parameters σ_j and ξ_j, both of the foregoing conditions are fulfiled in the wavelength range of interest, thus justifying the chosen treatment of roughness.

In Eq. (12), $D_j^z\sigma_j^2$ equals the power diffusely scattered at interface j. D_j^z are complicated functions of the index profile. Consequently, diffuse-scattering losses are determined not only by σ_j but also by the index profile. Anyway, the important thing to be noted is that losses at an interface depend greatly on the refractive-index contrast at that interface. The higher the contrast, or, which is equivalent, the reflectivity, of an interface the larger the amount of power diffusely scattered. Air/film is the most highly reflective interface, and also the roughest.[14] The main contribution to diffuse scattering coming from this interface, one can omit, in Eq. (12), the negligible contributions from the other two. The square dependence of $P^{z,\sigma}$ on σ_j lends further support to this approximation.

Taking this approximation into account, and applying a φ incoherence treatment to $P^{z,\sigma}$ to consider the effects of nonparallel interfaces and microstructure, we get

$$P(\Phi)=P_1(\Phi)+P_2(\Phi), \tag{13a}$$

where

$$P_1(\Phi)=P^z(\Phi)+\frac{1}{6}\frac{\partial^2 P^z(\Phi)}{\partial\varphi^2}\Delta\varphi^2 \tag{13b}$$

and

$$P_2(\Phi)=\left(D_1^z(\Phi)+\frac{1}{6}\frac{\partial^2 D_1^z(\Phi)}{\partial\varphi^2}\Delta\varphi^2\right)\sigma_1^2. \tag{13c}$$

In P_1 we recognize an absorption term and in P_2 a diffuse-scattering term. Both dissipative terms bear the indirect influence of the factors of normal inhomogeneity and φ incoherence, which in themselves are nondissipative.

B. Imperfection-induced effects on power-loss spectra

In this section, we demonstrate the effect the different inhomogeneity and dissipation factors have on power-loss spectra. We start by considering the effect of absorption for an entirely homogeneous film and next we consider the changes that occur on introducing normal inhomogeneity, φ incoherence, and surface roughness. As we shall see below, absorption and surface roughness are the factors that most crucially affect power-loss spectra. This is natural, as, unlike all other factors, they dissipate power.

The spectrum shown by the solid line in Fig. 3(b) demonstrates the effect of absorption for an entirely homogeneous film. The absorption coefficient $a(E)$ producing this spectrum is illustrated in Fig. 3(a). In the lower-energy region, the dissipative mechanism of absorption is very weak due to extremely small a, so $P\approx 0$. At higher energies, P increases since a increases. However, as well as this overall trend, one observes an oscillatory behavior. Unambiguously, the smooth and featureless energy dependence of a, by itself, could never explain such behavior. This is an interference-induced effect explained as follows.

In the absence of absorption, $\mathcal{E}_{\text{bound}}$, the amount of energy bound inside the film, is adjusted by the interference of waves that come and go between the air/film and the film/substrate interfaces. Because of constructive interference, $\mathcal{E}_{\text{bound}}$ is maximized at $\{\Phi=q\pi,\ q\in N\}$, while because of destructive interference it is minimized at $\{\Phi=q\pi+\pi/2,\ q\in N\}$. Upon introducing absorption, the more (less) $\mathcal{E}_{\text{bound}}$ is available in the film, the more (less) energy the absorption dissipates, In the higher-energy region, P reaches a plateau. In this region, due to large a, light penetrates only an epidermic slice near the air/film interface. Then it is well known that $P\approx 1-[(n-1)/(n+1)]^2$, where n is the refractive index of this epidermic slice. The observed plateau reflects just the constant n. As light penetrates a small distance inside the film, no light reaches the film/substrate interface. Thus no wave interference takes place and, consequently, no fringes appear.

The solid line in Fig. 3(b) changes into the dash-dotted line upon introducing normal inhomogeneity and φ incoherence. Either inhomogeneity factor is nondissipative on its

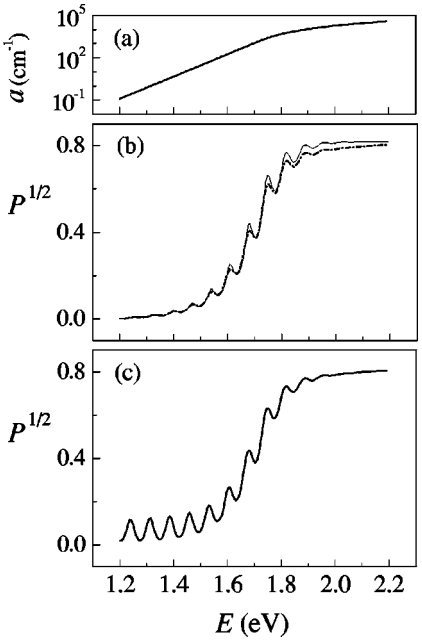

FIG. 3. The absorption coefficient shown in (a) is typical of a-Si:H and was employed in the calculation of the power-loss spectra depicted in (b) and (c). In (b), the solid line corresponds to an entirely homogeneous film and the dash-dotted line to an inhomogeneous film in which normal inhomogeneity and φ incoherence have been introduced. Surface roughness is absent. (c) corresponds to a fully inhomogeneous film. Normal inhomogeneity and φ incoherence as well as surface roughness are all taken into account. In all calculations the total thickness D, $D=D_{\mathrm{FIL}}+D_{\mathrm{bulk}}+D_{\mathrm{BIL}}$, as well as the average retractive index n, $n=(n_{\mathrm{FIL}}D_{\mathrm{FIL}}+n_{\mathrm{bulk}}D_{\mathrm{bulk}}+n_{\mathrm{BIL}}D_{\mathrm{BIL}})D^{-1}$, are taken to be identical: $n=3.7$ and $D=2.4\,\mu$m. The same is also true of the index of the substrate: $n_{\mathrm{subs}}=1.5$. The other input parameters are, in (b), dash-dotted line, $n_{\mathrm{FIL}}=4$, $n_{\mathrm{BIL}}=3.4$, $D_{\mathrm{FIL}}=D_{\mathrm{BIL}}=200$ nm, and $\Delta l=50$ nm; in (c) $\sigma_1=3$ nm with all other parameters identical to those of the dash-dotted curve of (b). Use of the square root of P was prompted by the intention to emphasize oscillations in the lower-energy region of (c). These oscillations are a distinctive sign of a selective, roughness-induced, diffuse scattering.

own, so when the only dissipative mechanism, namely, the absorption, becomes very weak, $P\approx 0$. This is the case in the lower-energy region, where the dash-dotted line coincides with the solid one. At higher energies, we observe small differences. The dash-dotted line appears to be shifted relatively to the solid, and its interference fringes are damped in comparison. Damping is due to φ incoherence and shift to normal inhomogeneity. Shift results in lowering of the plateau, evident in the higher-energy region. As we mentioned above, in this region, P depends only on the refractive index near the air/film interface. Thus the lowering of the plateau reflects just the different indices near the air/film interface for the two cases depicted.

One should note that power loss is little affected by introducing normal inhomogeneity and φ incoherence. This is especially true in the lower-energy region. This picture is in complete contrast with the picture we obtained about reflectance in Sec. II.

In the spectrum shown in Fig. 3(c), we consider the effect of surface roughness. In the intermediate- and higher-energy region, this effect is obscured by the effect of absorption. In

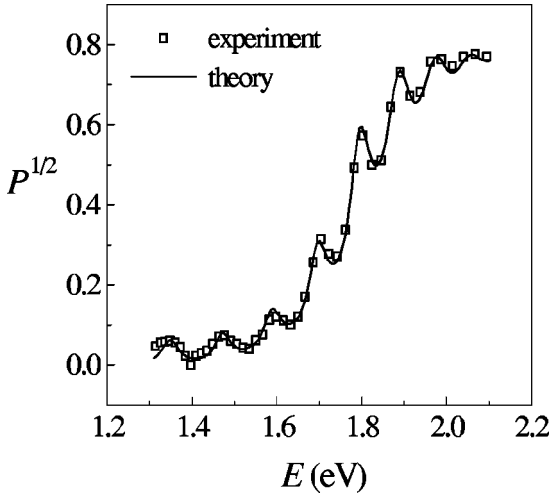

FIG. 4. Open squares show the experimental power-loss spectrum of a lightly boron-doped glow-discharge a-Si:H film. The thickness of the film is 1.2 μm. The solid line is the theoretical simulation. The input simulation parameters were obtained from analyzing the experimental spectrum in the way detailed in Sec. IV of the text. Use of the square root of P was prompted by the intention to emphasize oscillations in the lower-energy region. These oscillations are a distinctive sign of a selective, roughness-induced, diffuse scattering.

the lower-energy region, however, absorption is very weak and the effect is clearly visible. Evidently, surface roughness produces oscillations. This peculiar behavior is a clear sign of diffuse-scattering losses, which occur in a selective manner. According to the graph, diffuse scattering is maximized at $\{\Phi=q\pi,\ q\in N\}$, whereas it is minimized, almost vanishing, at $\{\Phi=q\pi+\pi/2,\ q\in N\}$. The physical interpretation underlying this interesting behavior is as follows. Diffuse scattering is produced by the *disorderly* positioning of the electric dipole moments which are induced at the *rough* surface of the air/film interface. The electric field of the electromagnetic radiation provides the necessary driving force that induces these moments. Due to wave interference inside the film, the amplitude of the electric field exhibits spatial oscillations. When $\Phi=q\pi$, the electric field amplitude takes a maximum value at the air/film interface, thus giving a considerable boost (large oscillation amplitude) to the dipole moments, which in turn produce a sizable diffuse-scattering effect. However, when $\Phi=q\pi+\pi/2$, the electric field amplitude almost vanishes at the air/film interface. Then the dipole moments are little activated (small oscillation amplitude), and, naturally, produce a negligible diffuse-scattering effect. This peculiar behavior gains in significance as it is corroborated by experiment. Figure 4 provides indisputable evidence on that point.

IV. EXTRACTION OF THE ABSORPTION COEFFICIENT

A. The optical method

In analyzing optical spectra to extract $a(E)$, it is a common practice to neglect imperfections and deal with an ideal specimen. Within the limits of this simplification, several methods have been proposed. Amongst them, the best seems to be that[18] employing the transmittance-maxima envelope

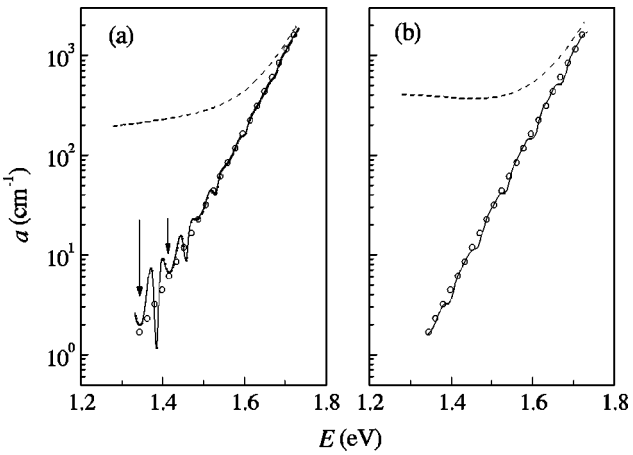

FIG. 5. (a) The solid line is the absorption coefficient extracted from analyzing the calculated power-loss spectrum illustrated in Fig. 3(c). Open circles demonstrate the true absorption coefficient that was used to generate the spectrum. The method of analysis is detailed in Sec. IV of the text. Intense fluctuations observed on the solid line in the lower-energy region demarcate the application limits of the method. The arrows show points at which the analysis-induced errors almost vanish (error-free points). The result of the conventional method of analysis, the dotted line, is given for comparison. (b) The solid line is the absorption coefficient extracted from analysis of the calculated power-loss spectrum depicted by the dash-dotted line in Fig. 3(b). Open circles and dashed line have the same meaning as in (a).

$T_{\max}$ to extract $a(E)$. $T_{\max}$ is highly sensitive to absorption. However, it is highly sensitive to all kinds of imperfections too. The former sensitivity constitutes a good reason for using the method. The latter, however, proves a serious handicap that greatly harms its efficiency, especially in the region of low absorption. This is clearly demonstrated in the two graphs of Fig. 5. In either graph, the dashed line is $a(E)$ obtained from applying the foregoing method to calculated optical spectra. Note the large deviation from the true absorption coefficient, the open circles. That deviation is due to the disregard of imperfections in the analysis. Evidently, the region most seriously affected is the region of low absorption. There, the dashed lines show a thoroughly false behavior by ending in long absorption tails. An identical false behavior is obtained from the analysis of experimental spectra also, as evident in Figs. 6 and 7.

On facing this problem, we developed an improved optical method, employing P instead of $T_{\max}$. This choice was prompted by a simple but important observation, which promised a beneficial simplification. The observation is that P, unlike $T_{\max}$, is little affected by normal inhomogeneity and φ incoherence. This is especially true in the critical region of low absorption. Indeed, noting that $T_{\max}\approx 1-R_{\min}$, in this region, Figs. 1 and 2 leave no doubt about the large effect on $T_{\max}$; on the other hand, Fig. 3(b) clearly shows a small effect on P. Thus, in employing P in the analysis of optical spectra, one is tempted to disregard normal inhomogeneity and φ incoherence. As we shall see in Secs. IV B and IV C, this beneficial simplification is of relatively low cost to the efficiency of the method.

Disregarding in Eqs. (13a)–(13c) the inhomogeneity factors in question, we deal with the following simplified expression for P:

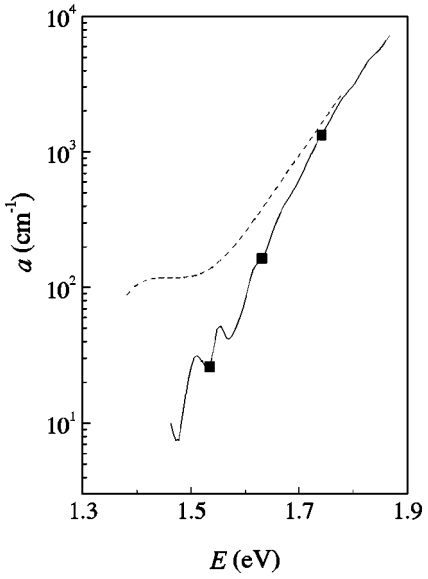

FIG. 6. The solid line is the absorption coefficient extracted from the analysis of the experimental power-loss spectrum depicted by open squares in Fig. 4. The method used is detailed in Sec. IV of the text. Error-free points are illustrated by solid squares. The result of the conventional method of analysis, the dotted line, is given for comparison.

$$P(E)=P^0(E)+D_1^0(E)\sigma_1^2, \tag{14a}$$

where

$$P^0(E)=P^0(n(E),a(E),n_{\text{subs}},D) \tag{14b}$$

and

$$D_1^0(E)=D_1^0(n(E),a(E),n_{\text{subs}},D). \tag{14c}$$

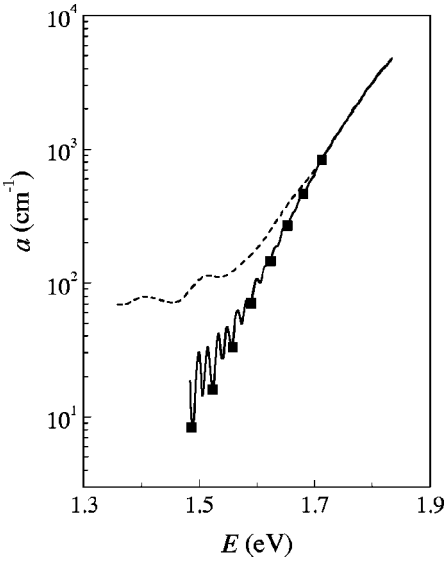

FIG. 7. The solid line is the absorption coefficient extracted from analyzing the experimental power-loss spectrum of an undoped glow-discharge a-Si:H film. The thickness of the film is 4 μm. The method of analysis is detailed in Sec. IV of the text. Error-free points are depicted by solid squares. The result of the conventional method of analysis, the dotted line, is given for comparison.

The superscript 0 denotes the complete absence of normal inhomogeneity. $P(E)$ depends on the following parameters: $n(E)$, the refractive index of the film; n_{subs}, the refractive index of the substrate; D, the thickness of the film; σ_1, the rms roughness at the air/film interface; and $a(E)$, the absorption coefficient. Note that the only imperfection taken into account is surface roughness at the air/film interface. In analyzing $P(E)$, n_{subs} is considered to be a known parameter as, in practice, it can always be measured *a priori* in a separate experiment. The remaining unknown parameters are determined as follows. In the first place, one calculates $n(E)$ and D by using a method[19] based on the equations governing interference extrema. Next, one calculates σ_1 from the amount of the power diffusely scattered. This amount is derived from Eq. (14a) by putting $a=0$. Noting that $P^0=0$ for $a=0$, we get

$$P(E)=D_1^0(n(E),n_{\text{subs}},D)\sigma_1^2. \tag{15}$$

As discussed in detail in Sec. III B and clearly demonstrated in Figs. 3 and 4, the diffusely scattered power is maximized at specific energy positions. By choosing the lowest-energy P maximum, which is safely free of any contributions coming from absorption, we calculate σ_1 through Eq. (15). Finally, the only unknown parameter left, namely, $a(E)$, is extracted by using Eq. (14a).

It is very important to notice that, in analyzing experimental data, the efficiency of this method crucially depends on the elimination of a systematic error from the measured reflectance. The latter is defined as the ratio of the measured flux reflected off the film to the measured flux incident on the film. The problem arises from the fact that incident and reflected fluxes reach the photodiode following different paths. Fluxes are directed toward and are finally focused on the active area of the photodiode by different sets of mirrors. Because of this, it is necessary to correct the measured reflectance by a factor taking into account the different reflectivities of the two mirror sets. By removing this systematic error, the previous $\pm 0.5\times 10^{-2}$ experimental error in P is reduced to $\pm 0.5\times 10^{-3}$. Note that the reflectance correction factor is wavelength dependent. The proper way to measure it will be presented elsewhere.[10]

B. Analysis of calculated optical spectra

Before analyzing experimental spectra, we test the efficiency of the method detailed in the previous section on calculated spectra. The power-loss spectrum of Fig. 3(c) is very appropriate. All of the normal inhomogeneity, φ incoherence, and surface roughness were taken into account in its calculation. Analysis of this particular spectrum produces the absorption coefficient depicted by the solid line in Fig. 5(a). The first positive indication is the significantly increased efficiency of this method as opposed to the inefficiency of the conventional method. Evidently, the solid line is much closer to the true absorption coefficient than the dashed line. The false absorption tail is removed. However, intense fluctuations, observed in the lower-energy region of the spectrum, demarcate the success limits of the method. These fluctuations are indisputably due to the disregard of normal inhomogeneity and φ incoherence in the analysis of the data. Let us recall that this simplification is made in P_1 and P_2, the two terms of Eq. (13a). One is then curious about whether the simplification made upon P_1 and the simplification made upon P_2 are both equally responsible for the artifact of the fluctuations. In order to find out, we analyze the spectrum depicted by the dash-dotted line in Fig. 3(b). Note that for this particular spectrum $\sigma_1=0$, or, which is equivalent, $P_2=0$. Since P_2 is missing, P_1 remains as the only term generating that spectrum. Analysis gives the absorption coefficient depicted by the solid line in Fig. 5(b). Evidently, the line is in excellent agreement with the true absorption coefficient, the open circles, within the entire energy range considered. That means that, as far as P_1 is concerned, the simplification of disregarding normal inhomogeneity and φ incoherence in the analysis is of no cost to the extracted $a(E)$. Thus, it is that same simplification, but imposed on P_2, that produces the artifact of the fluctuations. Note that this conclusion has a general value, as it was verified not only in the case considered here but in many different cases.

At certain points, shown by arrows in Fig. 5(a), very good agreement with the true absorption coefficient persists, despite fluctuations. At these points $\Phi=q\pi+\pi/2$, $q\in N$. As explained at the end of Sec. III B, diffuse scattering almost vanishes at these Φ values, thus implying that $P_2\approx 0$. Consequently, the reason for the artifact being missing, the error in the extracted a is missing. Note that at the specific Φ values the analysis gives excellent results by just treating the film as if it were ideal.

As well as $a(E)$, the analysis also estimates σ_1. The simplifications made introduce a small error of less than $\pm 10\%$ in its estimation.

C. Analysis of experimental optical spectra

The experimental power-loss spectrum, shown in Fig. 4 by open squares, was taken from measuring a slightly boron-doped a-Si:H film with thickness 1.2 μm. Analysis of this spectrum gives the absorption coefficient depicted by the solid line in Fig. 6. Evidently, all the features obtained in the analysis of calculated spectra are obtained again here. The overall linear dependence obtained between 10 and 10^3 cm^{-1} is indicative of good results. Fluctuations, clearly visible in the lower-energy region, are a sign of the presence of normal inhomogeneity and φ incoherence. To exclude the possibility of this artifact being merely a random effect produced by experimental noise, we repeated measurements. In analyzing them, we got again an identical a spectrum. This coincidence, being contradictory to the random nature of noise, excludes the possibility of noise being the origin of the artifact.

Regarding roughness, the analysis gives $\sigma_1=1.3$ nm. This value is in very good agreement with the true value $\sigma_1=1.2$ nm, which was measured by atomic force microscopy. Such a good agreement was obtained in all cases examined, σ_1 always deviating by less than $\pm 10\%$ from the true value.

An important prediction of the analysis finds experimental support in Fig. 7. The spectrum shown by the solid line is extracted from the analysis of data that were taken by measuring an undoped a-Si:H film with thickness 4 μm. Solid squares lie in positions where $\Phi=q\pi+\pi/2$, $q\in N$. Notice their extremely low scattering in comparison to the amplitude of the fluctuations themselves. They all lie in an almost

perfectly straight line. As explained in Sec. IV B, at $\Phi = q\pi + \pi/2$, $q \in N$, the extracted a is essentially error-free. In Fig. 7, the low scattering of the solid squares corroborates this very fact.

In the region extending from $a \approx 10$ cm^{-1} to $\alpha \approx 10^3$ cm^{-1}, that is, the Urbach region, the exponential character of the absorption edge gives rise to an important parameter that is a measure of the total disorder,[11] static and thermal, present in the film. This is the so-called Urbach parameter E_0. The sharper the absorption edge, the smaller E_0, and, in turn, the smaller the disorder present in the film. In the Urbach region, by applying linear regression to $\ln a(E)$, we derive E_0 from the slope of that linear regression: $E_0 = (\partial \ln a/\partial E)^{-1}$. As evident in Table I, artifacts induce a small uncertainty in the derived E_0. The most accurate value is expected when the linear regression considers only the error-free points at $\Phi = q\pi + \pi/2$, $q \in N$. This is possible as long as the film under investigation is not too thin, $D \gtrsim 1.5\,\mu$m. Then the number of error-free points detected within the Urbach region is sufficiently large ($\geqslant 3$) to make it feasible for linear regression to apply.

In order to assure indisputable evidence of the efficiency of the current method, we compare its results with those of photothermal deflection spectroscopy (PDS) as well as those of the constant photocurrent method (CPM). It should be noticed that the CPM and PDS are also not free from artifacts.[20,21] These artifacts, again manifested as fluctuations in the extracted $a(E)$, are averaged out[20] in order to give a smoother curve. Given that the CPM and PDS are normalized to the optical measurement in the high-absorption region, E_0 provides a safe criterion of comparison. As evident in Table I, our optical method is in good agreement with both the CPM and PDS.

TABLE I. E_0 (meV) derived in order to compare the current optical method (COM) with PDS and CPM. In deriving E_0 from the COM we use (a) the full a-spectrum between 10 and 10^3 cm^{-1}, (b) only the error-free points detected within the same range.

	Method			
	COM		PDS	CPM
Film	(a)	(b)		
Boron-doped a-Si:H	56	53		54
Undoped a-Si:H	53	47	49	

ACKNOWLEDGMENTS

The author thanks Professor Helmut Fritzche and Professor Pere Roca i Cabarrocas for providing the films measured, and Professor Petros Ditsas for useful comments on the final presentation of this paper.

[1] E. Chason and T. M. Mayer, CRC Crit. Rev. Solid State Mater. Sci. **22**, 1 (1997).
[2] J. M. Eastman, Phys. Thin Films **10**, 167 (1978).
[3] Z. Knittl, *Optics of Thin Films* (Wiley, New York, 1976).
[4] H. E. Bennet and J. M. Bennet, Phys. Thin Films **4**, 12 (1967).
[5] R. Swanepoel, J. Phys. E **17**, 896 (1984).
[6] N. M. Amer and W. B. Jackson, in *Semiconductors and Semimetals*, edited by J. I. Pankove (Academic, Orlando, FL, 1984), Vol. 21B.
[7] M. Vanecek, J. Kocka, J. Stuchlik, and A. Triska, Solid State Commun. **39**, 1199 (1981).
[8] S. Nonomura, H. Hayashi, and S. Nitta, Rev. Sci. Instrum. **60**, 657 (1989).
[9] P. Stradins, H. Fritzsche, and M. Tran, in *Amorphous Silicon Technology—1995*, edited by M. Hack, E. A. Schiff, M. Powell, A. Matsuda, and A. Madan, MRS Symposia Proceedings No. 377 (Materials Research Society, Pittsburgh, 1995), p. 467.
[10] A. Kondilis and P. Tzanetakis (unpublished).
[11] G. D. Cody, in *Semiconductors and Semimetals* (Ref. 6).
[12] G. Muller, F. Demond, S. Kalbitzer, H. Damjantschitsch, H. Mannsperger, W. E. Spear, P. G. Le Comber, and R. A. Gibson, Philos. Mag. B **41**, 571 (1980).
[13] B. Harbecke, Appl. Phys. B: Photophys. Laser Chem. **39**, 165 (1986).
[14] Typical surface parameters of glow-discharge a-Si:H films measured by atomic force microscopy: At the air/film interface $\sigma_1 = 2$ nm and $\xi_1 = 150$ nm; at the substrate/air interface $\sigma_3 = 0.6$ nm and $\xi_3 = 100$ nm. σ is the rms height of surface irregularities and ξ the autocorrelation length. Even though the film/substrate interface cannot be directly measured, it is reasonable to assume that it retains the surface morphology of the naked substrate, i.e., $\sigma_2 \approx \sigma_3$ and $\xi_2 \approx \xi_3$.
[15] E. C. Freeman and W. Paul, Phys. Rev. B **20**, 716 (1978).
[16] M. Vanecek, J. Holoubek, and A. Shah, Appl. Phys. Lett. **59**, 2237 (1991).
[17] At $E = 1.2$ eV, the volume-scattering extinction coefficient a_s ranges[16] between 1 and 3 cm^{-1}. Such small values induce very small power losses in diffuse scattering. For a film with thickness $D = 4$ μm and for $a_s = 3$ cm^{-1}, the loss of power is $P_s \approx a_s D = 1.2 \times 10^{-3}$. The noise-induced error in our measurements is $P_{\text{noise}} = \pm 0.5 \times 10^{-3}$. Thus, we are talking about nonmeasurable volume-scattering losses.
[18] D. Goldschmidt. J. Opt. Soc. Am. A **1**, 275 (1984).
[19] R. Swanepoel, J. Opt. Soc. Am. A **2**, 1339 (1985).
[20] C. B. Roxlo, B. Abeles, C. R. Wronski, G. D. Cody, and T. Tiedje, Solid State Commun. **47**, 985 (1983).
[21] A. Fejfar, A. Poruba, M. Vanecek, and J. Kocka, J. Non-Cryst. Solids **198-200**, 304 (1996).